Genesis of MoS2 from Model-Mo-Oxide Precursors Supported on γ-Alumina

Amit Sahu, Stephan Steinmann, Pascal Raybaud

Genesis of MoS_2 from model-Mo-oxide precursors supported on γ-alumina

*Amit Sahu, [†§] Stephan N. Steinmann,[§] and Pascal Raybaud[†§]**

[†] IFP Energies nouvelles, Direction Catalyse et Séparation, Rond-Point de l'Échangeur de Solaize, BP 3, 69360 Solaize, France.

[§] Univ Lyon, ENS de Lyon, CNRS UMR 5182, Laboratoire de Chimie, F-69342 Lyon, France.

* Corresponding author: Pascal Raybaud, email : pascal.raybaud@ifpen.fr , phone: +33.4.37.70.23.20

ABSTRACT: The molecular-scale understanding of the genesis of the MoS_2 phase from Mo-oxide precursors by sulfo-reduction supported on alumina is highly challenging with a strong impact on the activation process of heterogeneous industrial catalysts. By means of density functional theory (DFT), we quantify the activation free energies of the elementary steps involved in the sulfo-reduction mechanisms of Mo-trioxide oligomers and the stability of the corresponding Mo-oxysulfide intermediates supported on the γ–alumina (100) surface. The Gibbs free energy profiles highlight the characteristic chemical reactivity of various oxygen sites involved in the O/S exchange mechanism and reveal that that interfacial oxygen atoms (Mo-O-Al) are the most challenging sites to be exchanged with S. We quantitatively compare the two main paths proposed experimentally: the one involving Mo-oxysulfide and Mo-trisulfide intermediates and the second one involving only Mo-oxysulfide. While O/S exchange requires moderate activation energies, the rate-determining steps correspond to S- and O-removal on small $Mo_nO_{3n-x}S_x$ or Mo_nS_{3n} ($n \leq 3$) oligomeric intermediates. To overcome these high energy steps, the small Mo-trisulfide (Mo_nS_{3n}) oligomers are proposed to be fast diffusing surface species and to promote the growth process towards the targeted MoS_2 phase. A reconstruction from chain to triangular Mo_3S_9 conformer also facilitates this phase transformation.

KEYWORDS: MoS_2 catalyst, γ–alumina, activation, sulfidation, reduction, diffusion, growth, Mo-oxide, oxysulfide, MoS_3, density functional theory, mechanism.

1. Introduction

MoS_2 based materials represent a wide interest for various catalytic and electrocatalytic applications such as hydrodesulfurization process, hydrogen evolution reaction, etc. However, the catalytic performances strongly depend on the sulfidation state of Mo resulting from the preparation steps.[1] More particularly, the final activation step is crucial for the genesis of the targeted disulfided Mo active phase from its Mo-oxide precursors deposited on a support (such as γ–alumina (γ–Al_2O_3),[2–4] anatase-TiO_2,[5] amorphous silica (SiO_2),[6] and amorphous silica-alumina)[5] after impregnation, drying, or calcination. This activation involves a sulfo-reduction process with either H_2/H_2S gas phase (laboratory scale) or organo-sulfur compounds in a liquid phase (industrial scale) at elevated temperature (350°C).[1,7–9] In the latter case, the sulfidation starts only after the liquid organo-sulfur compound decomposed into H_2S.[8,10–12]

Therefore, to improve the resulting properties of these catalysts, it remains critical to better understand at a molecular scale how the MoS_2 active phase is engendered from its oxide precursors. Even though the activation step of γ–alumina supported molybdenum oxide precursor by sulfo-reductive treatment has been the subject of many spectroscopic studies,[13–18] several mechanistic questions remain open regarding the nature of the Mo-oxysulfides (MoO_xS_y) and Mo-trisulfide (MoS_3) intermediates, the reaction pathways, and the kinetically limiting steps (**Figure 1**).

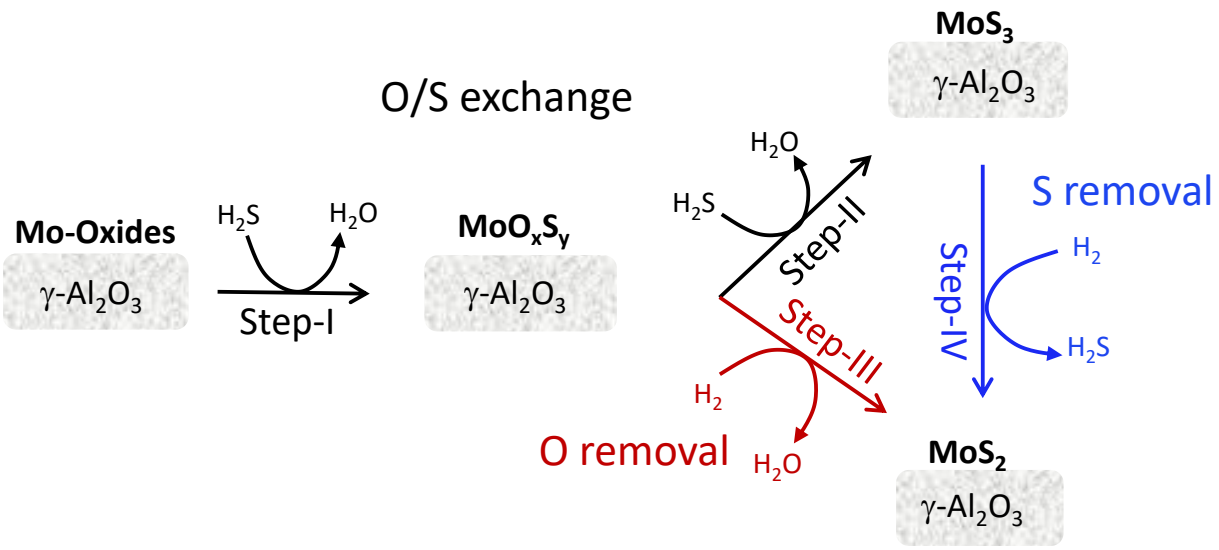

Figure 1. Schematic diagram of sulfidation of Mo-oxide precursors by H_2S into Mo oxysulfides (MoO_xS_y), and from oxysulfides to MoS_2 following two pathways: direct reduction to MoS_2 by H_2 (steps I and III) or sulfidation into MoS_3 followed by transformation to MoS_2 (steps I, II and IV).

The oxidation state of Mo changes from VI, to V and IV during the activation process, corresponding to widely invoked MoO_xS_y[7,15,16,19,20] and MoS_3[15,17,18,21–24] intermediates. These intermediates are complex amorphous compounds often well dispersed on γ-alumina. Identifying molecular structures for these amorphous compounds remains challenging. For instance, a wide structural diversity exists for the MoS_3 polymorphs as a function of size even without support effects.[25] The structural insights for Mo oxysulfides is even more elusive, particularly in the presence of the alumina support.

Considering the respective role of H_2S and H_2 as potential reactants during sulfo-reduction of alumina-supported Mo-oxide, H_2 consumption was observed at high temperature only during temperature-programmed reduction (TPR). At the same time, H_2S uptake was seen at low

temperatures in temperature-programmed sulfidation (TPS).[7,19,20] Furthermore, it has been shown that H_2S is the key reactant to allow the formation of the MoS_2 phase even without H_2 uptake at an early stage.[7,19,20,24,26] In a second stage, the observed release of a substantial quantity of H_2S may feature the conversion of Mo-trisulfide intermediates into Mo-disulfide phase through H_2 reduction.[15–18,21,23] Therefore, if the MoS_3 intermediate is involved, the activation process is proposed to occur in two stages: O/S exchange with H_2S[20,27] leading to the MoS_3-phase[15,24,28] from MoO_3-like species (steps I and II in **Figure 1**), followed by its transformation to MoS_2 phase thanks to H_2 reduction (step IV). However, at this stage, the possibility of direct reduction of oxysulfide to disulfide phase cannot be (step III) ruled out. For these reasons, our study will focus on the key role of H_2S only as sulfiding agent in steps I, II, and by considering the possible role of H_2 at a latter stage in steps III and IV.

Thus, identifying and characterizing Mo-oxysulfides intermediate remains crucial but challenging from an experimental point of view. In particular, in situ EXAFS enabled to follow the evolution of bond lengths such as Mo-O, Mo-S, Mo-Mo[8,17,18] and to reveal some key intermediates such as MoO_xS_y and MoS_3. Time-resolved XAS and Raman spectroscopy on Ni promoted MoS_2 catalyst supported on Al_2O_3 provided critical insights on such intermediates by chemometric multivariate curve regression with altering least-squares (MCR-ALS) method.[29] Interestingly, the molecular models of MoO_xS_y intermediates proposed by EXAFS are constituted from dimeric or trimeric Mo clusters. The XAS analysis also enabled to distinguish specific Mo-oxysulfide intermediates depending on gas phase or liquid sulfidation protocol.[8] Another interesting trend revealed by in-situ XAS is that during liquid phase sulfidation, the delayed sulfidation temperature induces a depolymerization of the polyoxomolybdate precursor between 80 to 230°C.[8] Hence, small Mo-oxide oligomers (as small as dimers or trimers) highly

dispersed on the support are formed and will be the relevant oxide species involved in sulfidation. For that reason, as also explained in what follows, we will consider such small Mo-oxide oligomers as the starting species for the simulation of sulfo-reduction mechanisms.

Also, the disappearance of some characteristic top oxo-species Mo-O_t and the appearance of S_2^{2-} and S^{2-} species was analyzed as a function of temperature by in situ Laser Raman Spectroscopy for alumina supported Ni-promoted MoS_2 catalyst.[18] Temperature-dependent infra-red (IR) emission spectrum of sulfidation of crystalline MoO_3 showed that around 100-200 °C, the peak of bridging oxo-species Mo-O-Mo disappears, and a new peak assigned to top oxo-species Mo=O_t appears before Mo-S formation. Then, on Mo-oxysulfides, the Mo=O_t species disappear more rapidly than Mo-O-Mo species.[16] This analysis also seems to differentiate the behavior of bulk crystalline MoO_3 from the one dispersed catalyst.

Lastly, transmission electron microscopy (TEM) highlighted that the sulfidation process occurs through a layer-by-layer growing process involving the diffusion of presumably small Mo-oxysulfides or sulfides species on the support.[30] The nature and role of such small Mo-entities remain to be elucidated.

Very few density functional theory (DFT) studies addressed the sulfidation process of Mo-oxide supported on alumina. Some DFT investigations analyzed the interactions of Mo, or W-oxide clusters of various sizes support by Al_2O_3,[31,32] TiO_2,[33–36] and SiO_2.[37] Several plausible mono-oxo and di-oxo Mo centers were proposed for Mo_1O_3, and Mo_2O_6 species on γ-alumina (100) and (110) surfaces using DFT calculations.[31,32] DFT was also applied to investigated the stability and interaction mode of the final sulfided MoS_2 clusters on γ–alumina and TiO_2 surface, revealing Mo-O-Al(Ti) chemical bridges.[38,39] Also, the thermochemistry of sulfur-oxygen exchange at the edges of the MoS_2 nano-crystallite to identify the possible residual

Mo-O chemical bonds after sulfidation using DFT suggested that the MoS_2 edge is the most difficult to sulfide and maybe the location of residual oxidized Mo sites.[40] Similarly, the sulfur/oxygen exchange was predicted to occur in the long-run on the MoS_2 edges under electrocatalytic conditions such as hydrogen evolution reaction (HER).[41]

The dissociative adsorption of H_2S was investigated on multilayers of the α-MoO_3 phase deposited on two different γ-alumina models by using DFT. The reactivity of the monolayer of MoO_3 deposited on the surface of non-spinel γ-alumina was shown to be highest due to charge transfer from alumina to the MoO_3 monolayer.[42] Other quantum simulation studies attempted to rationalize the O/S exchange thermodynamics of bulk,[43] monolayer or large clusters of MoO_3.[44–46] In general, it was found that replacing the terminal oxo-site by sulfur is more feasible (through vacancy formation) and exothermic in nature than the O/S exchange for bridging (two fold) or tridentate oxygen sites. Moreover, O-vacancy creation increases the reactivity of sulfiding agents (H_2S or S_2), which means that the use of hydrogen would enhance the sulfidation rate. As more terminal oxygens are being replaced by sulfur, they can form S-dimers leading to a stabilization of the system.[45] Thermodynamic trends in thiolysis energies of Mo oxide precursors as a function of various supports (including alumina) analyzed by DFT calculations on small molecular clusters showed an appealing correlation between thiolysis energy descriptor and sulfidation degree and/or dispersion,[47] although no kinetic analysis was provided by this study and the realism of the small cluster models remains questionable.

However, to the best of our knowledge, no DFT study addressed the sulfo-reduction mechanisms of Mo-oxides dispersed on a support such as γ–alumina. Hence, numerous open questions remain about the molecular mechanisms and key oxysulfides intermediates involved in the elementary steps of **Figure 1,** such as O/S exchange, S-removal, O-removal involved during

activation. In particular, it would be crucial to identify the most refractory oxygen sites with respect to sulfidation, and the role of the Mo-trisulfide invoked by numerous experimental studies.

We have chosen to consider the sulfidation of small Mo_nO_{3n} oligomers (n=1, 2, and 3) deposited on the (100) γ–alumina surface since this surface have been suggested to have a higher degree of sulfidation than other planes of alumina.[48,49] The Mo_nO_{3n} oligomers have been suggested to be present on numerous oxide support (including alumina)[50–57] under various thermal conditions. Moreover, the Mo-oxysulfides intermediates formed in the course of sulfidation are also reported by EXAFS analysis to exhibit a very small Mo-Mo coordination number corresponding to such dimers or trimers.[19,29] As mentioned before, small Mo-oxides oligomers result from the depolymerization of polyoxomolybdates in high-temperature liquid phase sulfidation.[8] Finally, Mo-oxide trimers supported on alumina exhibit various types of O-species (top-oxo, bridging oxo, O-interfacial). These O-sites might feature characteristic reactivities towards H_2S and H_2, informing about the most O/S exchange-resisting sites encountered in the real experimental system.

We will thus investigate the interaction of small Mo-trioxide precursors with alumina and their sulfidation using H_2S and H_2 as key reactants. We will address the kinetic and thermodynamic aspects of sulfo-reduction and corresponding Mo-oxysulfide or trisulfide intermediates along the main path depicted in **Figure 1**. Finally, we will also discuss the effect of size, diffusion, and growth during this whole process.

2. Computational details

For all total energy calculations, density functional theory (DFT) as implemented in VASP[58–60] has been used relying on the Perdew-Burke-Ernzerhof (PBE)[61] functional within the framework of generalized gradient approximation (GGA). The long-range London dispersion interactions were included through a density-dependent dispersion correction (dDsC).[62,63] The projector augmented-wave (PAW) method[64] was chosen to describe the electron-ion interaction. The kinetic energy cut-off for the plane-wave basis set has been fixed at 400 eV. For the minimization of the electronic energy, Gaussian smearing with a width of 0.2 eV was chosen.

A mixture of the blocked-Davidson scheme and residual minimization method direct inversion in the iterative subspace has been applied. Spin-polarized calculations were performed to obtain the ground state of the clusters. By scrupulously varying the difference of two spin components, we examined the spin effect, but the ground states remained nonmagnetic. Electronic convergence was assumed to be achieved at 10^{-6} eV. For geometry optimization, the conjugate gradient algorithm was used. Geometric convergence cut-off has been set to 0.02 eV/Å.

For frequency calculations, the structures have been optimized with tighter convergence criteria: 10^{-7} eV for electronic properties and maximum gradients below 0.01 eV/Å. The finite difference method has been used to calculate the frequencies and the density functional perturbation theory (DFPT) method to simulate the infra-red (IR) spectra within the framework of dipole approximation as implemented in VASP.[65–67] For systems where both methods have been applied, they are found to give consistent results. To avoid the peaks from alumina support, we have only simulated the modes concerning the cluster and bonded or weakly interacting part of underneath alumina.

For determining the reaction energy (ΔE) of various reaction steps on alumina at 0 K, the following formal equation was used:

$$\mathbf{\Delta G = G(P_{surface}) + G\left(P_{gas}\right) - G(R_{surface}) - G(R_{gas})} \quad \textbf{(1)}$$

where $\mathbf{G(R_{surface})}$ (respectively $\mathbf{G(P_{surface})}$) is the Gibbs free energy of the reactant (respectively product) adsorbed on the "catalytic surface", and $\mathbf{G\left(R_{gas}\right)}$ (respectively $\mathbf{G\left(P_{gas}\right)}$) is the Gibbs free energy of the reactant (respectively product) in the gas phase. The detailed equations of each considered reaction are reported in **Supporting Information S1**.

This study focused on the (100) surface of γ-alumina (**Figure S1**). This slab has been constructed following the procedure by Digne et al.[68,69] according to the bulk alumina model defined by Krokidis et al..[70] Moreover, it has been shown that in sulfur-reduction conditions as encountered in this work, the surface remains dehydrated and is not sulfided.[71] We have relaxed the first two layers of the surface, and the bottom two layers have been kept fixed.

Once the most stable adsorption sites for the Mo-oxide clusters are identified on the surface, we assume that the adsorbed cluster will not move or diffuse on the surface in the course of the sulfo-reduction mechanism. This assumption is based on the strong Mo-oxide or Mo-oxysulfide support interaction shown later in the results. This does not exclude that locally the anchoring sites evolve as a function of sulfidation.

During these sulfo-reduction steps into the final disulfides, we identify the limiting steps and corresponding activation energies. To determine the activation energy, we computed the energy of the transition state (TS). We used the Nudged Elastic Band (NEB) method in conjunction with constrained force-based optimizers to determine the geometry of the transition states (TS).[72–75] To generate the intermediate images between reactant and product, we used the Opt'npath

open-source code.[76] We performed the frequency calculations to confirm TS as a first-order saddle point on the potential energy surface with only one imaginary frequency, and that the imaginary mode corresponds to the restoring force along the direction from the TS to the reactant or product. We have used an open-source code to trace the reaction energy plots.[77]

All aforementioned electronic energies were corrected by the contribution of zero-point energy, thermal corrections at T=623K (experimental temperature for sulfo-reduction), and entropy corrections in order to determine the vibrational free energy:

$$\boldsymbol{\Delta G = \Delta H - T\Delta S} \quad \mathbf{2}$$

$$\mathbf{\Delta H = \Delta U + P\Delta V} \quad \mathbf{3}$$

$$\mathbf{\Delta U(S) = \Delta U(S)_{ele} + \Delta U(S)_{vib} + \Delta U(S)_{rot} + \Delta U(S)_{trans}} \quad \mathbf{4}$$

We assumed that the Mo_nO_{3n}, $Mo_nO_xS_{3n-x}$, and Mo_nS_{3n} oligomers are immobile on the alumina surface due to their strong chemical anchorage. We included the translational and rotational U(S) contributions for the gas-phase molecules H_2O, H_2S, and H_2.

All free energy diagrams are plotted for 1 bar partial pressure of H_2O, H_2S, and H_2. It is possible to include a correction on the thermodynamic reference levels of these molecules in gas phase induced by pressure effects as described in **Supporting Information 1.**

3. Results

3.1. Interaction of molybdenum oxides precursors with γ-alumina

Based on the experimental insights described in the Introduction, we first explore the stability of monomeric (Mo_1O_3), dimeric (Mo_2O_6), and trimeric (Mo_3O_9) Mo-oxides dispersed on alumina. To determine the optimal interaction and the adsorption sites of γ-alumina, we systematically explored the energetic stability of these species on the (100) γ-alumina surface.

For Mo_1O_3 and Mo_2O_6, our results (**Supporting Information 3.1)** are mainly consistent with previous theoretical works.[31,32] The Mo_3O_9 oligomer may exhibit two conformers in the gas phase: either cyclic or chain-like (**Figure-S2 c and d**), similar to the Mo_3S_9 (Mo-trisulfide) cluster where the chain and triangular conformers are competing.[14,21,25,78–83] The cyclic conformer is more stable than the chain by about 0.86 eV in the gas phase (**Figure S4**), similar to our previous finding for Mo_3S_9 clusters.[25] However, the strong support effect induces an inversion of the relative stability of the two conformers: the chain conformer becomes more stable by -0.42 eV on the (100) γ–alumina surface (**Figure S6)**. The same support effect is also observed for Mo_3S_9 clusters, as discussed later. The support interaction enables the formation of new Mo-O-Al and Mo-O_{surf} bonds, which cauterizes the under-coordination of Mo-atoms in the chain and leads to a square-pyramidal environment for each Mo-atom (**Supporting Information 3.2**), while in the absence of support, the Mo atoms are all stabilized in the tetrahedral environment by Mo-O-Mo cyclization (**Figure S2**). This interaction with support also impacts the nature of oxygen atoms which will be involved in the sulfur/oxygen exchange process, as described in the following.

Figures 3 and **S6** highlight the four distinct types of oxygen atoms present in the supported Mo_3O_9 (chain or cyclic): terminal oxo-species (O_t), bridging (O_{br}), interfacial-bidentate ($O_{int(bi)}$), and interfacial-tridentate ($O_{int(tri)}$). Terminal oxo-species (O_t) are connected to one Mo center only, while bridging oxo- (O_{br}) are bonded to two Mo-atoms (Mo-O-Mo). Interfacial-bidentate ($O_{int(bi)}$) are initial (gas phase) terminal oxo- that also interact with the aluminum site of support, becoming bridging species (Mo-$O_{int(bi)}$-Al). Interfacial tridentate ($O_{int(tri)}$) are initial bridging oxo- that also becomes bonded to aluminum sites of support 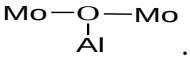

. We found two competing Mo_3O_9 chain conformers (**Figure S6a** and **S6b**), but we will discuss in the main text only the

most relevant one (**Figure S6a**) based on the sulfidation thermodynamics and kinetics consideration. This chain conformer exhibits two-terminal oxo (O_t) species, three bridgings (O_{br}), three interfacial bidentates ($O_{int(bi)}$), and one interfacial tridentate ($O_{int(tri)}$). All three Mo-atoms are penta-coordinated but possess distinct geometrical orientations. The central Mo-atom has an octahedral vacancy site; however, the terminal Mo-atoms have distorted square-pyramidal conformation. The details of the second conformer are given in **Supporting Information 3.2**. The analysis of the local environment of Al and O sites on Mo_nO_{3n} oligomers (n=1, 2, and 3) is compatible with earlier experimental ones proposed for various catalytic systems (not only HDS), where molybdenum oxides are found in a highly dispersed form on various oxide surfaces and could even exist as isolated MoO_x species after thermal treatment.[19,50–57]

3.2. Oxygen/sulfur exchange for Mo_3O_9 on alumina

Thermodynamic considerations

The supported oxide oligomers are expected to undergo a sulfo-reduction process to form Mo-oxysulfides or Mo-trisulfides intermediates, followed by their further transformation (reduction) to the final Mo-disulfide phase. The cyclic conformers remain more stable in the gas phase than the chain along the entire sulfidation path leading to the trisulfide phase (**Figure S3** and **S4**). By contrast, this trend is again reversed by the support. As explained in detail in Introduction, numerous published experimental works underlined the key role of H_2S during the early stage of sulfo-reduction of Mo-oxide, we will thus assume here that hydrogen will not react at the first steps (I and II). Instead, we consider first that O/S exchange by H_2S adsorption and H_2O removal is thermodynamically preferred (as illustrated in what follows), which is in line with the earlier proposal by Muijsers et al.[28] Moreover, using H_2S is also coherent with some experiments that

reported MoS_2 formation under pure H_2S environment.[24,26] Note that we preliminary found that the direct reduction of Mo_3O_9 by hydrogen is endothermic (0.2 eV – 1.76 eV for first oxygen removal (**Supporting Information 5.3**) and 0.51 eV – 1.89 eV for the second oxygen removal). Thus,

We systematically examined the O/S exchange for multiple models: monomer, dimer, trimer (chain and cyclic) according to the various types of oxygen sites identified. Detailed results are reported in **Supporting Information 4, 5, and 6**); we present in what follows two thermodynamically relevant paths (path-1 and -2) for the chain Mo_3O_9 conformer. The O/S replacement on path-1 occurs more homogeneously than on path-2 (**Figure 2** and **Figure S8**). The first two steps of path-1 and path-2 are similar and involve bridging O-sites in O/S exchange. However, the main difference arises at the third and fourth steps where path-1 replaces the terminal oxygen, while path-2 replaces the interfacial ($O_{int(bi)}$). On path-1, the three Mo-atoms become all partially sulfided (connected to one S-atom) at $Mo_3O_6S_3$, whereas on path-2, only two Mo-atoms are sulfided at $Mo_3O_6S_3$.

Figure 2 reveals that the overall trend is exergonic. Even though step three is slightly less favored for path-2, the free energy gain at the 4^{th} step for path-2 becomes more significant, about -0.8 eV (**Figure 2**). This enhanced stability comes from the formation of S_2-dimer replacing two adjacent $O_{int(bi)}$ by S. Interestingly, such S_2 dimers are observed experimentally (see the forthcoming spectroscopic analysis). Path-1 favors the replacement $O_{int(bi)}$ and $O_{int(tri)}$ after the bridging and terminal oxygen. At the 7^{th} step, path-1 can be linked to path-2 by dissociating the half-bridged dimer formed at step 6 and creating a new S_2 dimer at step 7. The formation of new terminal S_2 dimer results in -0.5 eV stabilization. This observation is consistent with an earlier

DFT study of MoO_3 O/S exchange, where the S_2-dimer formation results in ~0.5 eV further stabilization.[45]

We thus propose that both paths co-exist or that a mixed solution combining path-1 until step 7 and a transition to path-2 after step 7 will lead to the formation of the most stable chain-Mo_3S_9. **Figure S12** highlights that the second chain conformer (**Figure S6b**) is actually slightly less stable on the sulfidation path, justifying our choice to focus on the chain conformer of **Figure S6a** only.

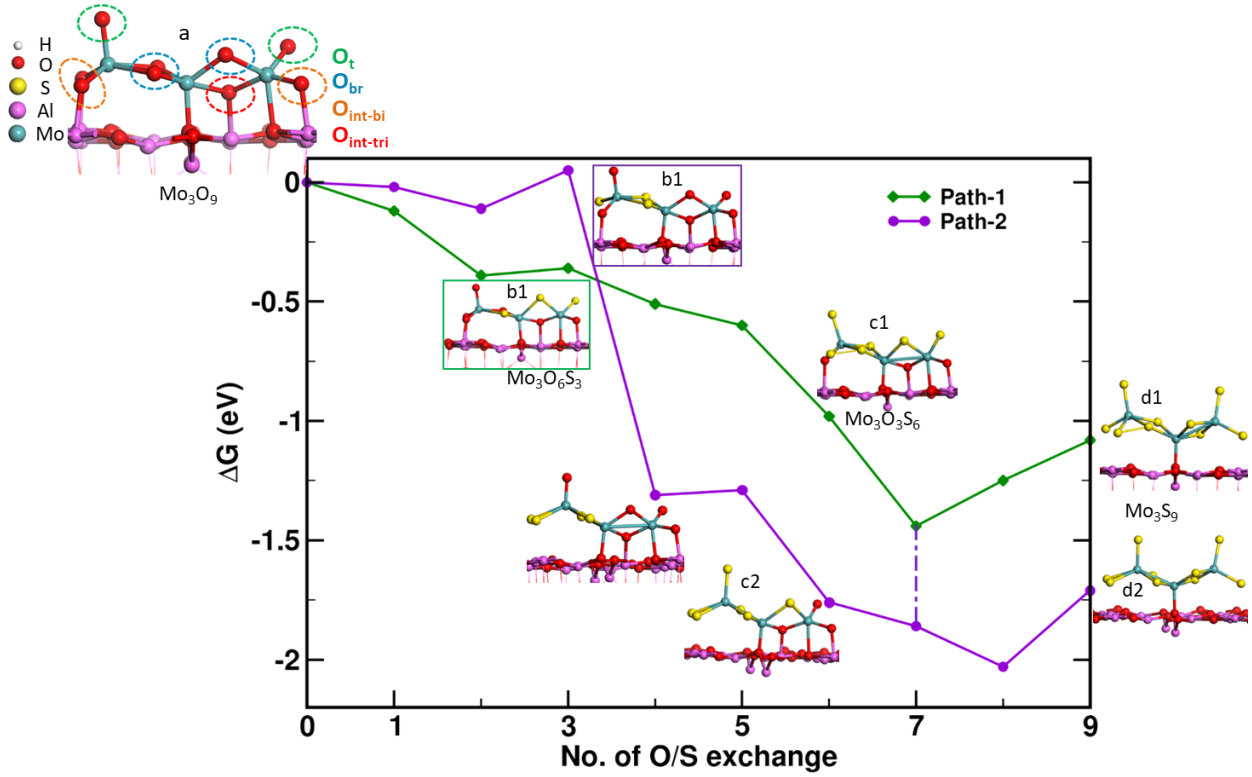

Figure 2. Gibbs free energy at 625 K for the O/S exchanges of chain-trimer Mo_3O_9 according to path-1 and path-2 using the alumina adsorbed Mo_3O_9 as reference. The possible transition between path-1 to path-2 is shown at step 7 by the vertical broken lines.

The O/S exchange energies of bridging and terminal oxygens are very similar from a thermodynamic aspect, whereas exchanging $O_{int(tri)}$ site costs ~0.65 eV additional energy. Except for the last few steps, every O/S exchange is exergonic by about -0.2 eV to -0.5 eV. Interestingly, this observation remains valid across the size and models (**Figure-S12**). This trend suggests that the last few O/S exchanges involving $O_{int(tri)}$ or $O_{int(bi)}$ are thermodynamically more arduous than earlier ones.

Structural and vibrational analysis of key intermediates

During the O/S exchanges, the local chemical and structural environment of $Mo_3O_{9-x}S_x$ intermediates evolve, involving the disappearance of Mo-O bonds and the simultaneous formation of new Mo-S and S-S bonds as highlighted by the evolution of Mo-O(S) bond lengths and coordination number of the critical intermediates in **Figure S9** where a comparison with EXAFS data is also given.[16–19,84] As detailed in **Supporting Information 5.2**, the DFT optimized structural values are consistent with EXAFS ones, and the calculations recover the various Mo-O bond lengths as a function of the type of O site.

The homogeneous path-1 involves the replacement of terminal and bridging oxygen first and later the interfacial ones ($O_{int(tri)}$ and $O_{int(bi)}$), while the heterogeneous path-2 exchanges the two bridging species followed by two $O_{int(bi)}$ out of three, then terminal ones, and finally $O_{int(tri)}$ and $O_{int(bi)}$, respectively (**Figure 2** and **Figure S8 b and c**). These oxysulfides contribute to the emerging Mo-S bonds as more oxygens are replaced by sulfur from $Mo_3O_6S_3$ and $Mo_3O_3S_6$ (**Figure S9 and S10**). For instance, new terminal Mo-S bonds of 2.14 Å (2.24 Å)[18] and Mo-S-Mo bonds of 2.41 Å (2.38 Å)[18] appear and are evidence of the presence of different S species such as S_2^{2-} and S^{2-} as also confirmed by IR/Raman,[16,18,21] while Mo-O_t vanishes as more S

replaced the oxygen (**Figure S9 and S10**). Moreover, since EXAFS revealed that a short Mo-O_t bond is still present in late oxysulfides intermediates,[17,18] the path-2 where sulfidation occurs heterogeneously from one side, may explain that the remaining terminal oxo species until $Mo_3O_3S_6$, as seen in EXAFS spectrum for short Mo-O bond. The Mo-Mo bond shrinks from 3.31 Å to 2.86 Å as more O/S exchanges take place.

To further assess the reliability of our Mo-oxysulfide intermediates, we also undertook a similar analysis by simulating the IR spectrum of each intermediate and compared them with available experimental data (**Figure-S10**). Various Mo-O stretching modes were recovered between 700-1000 cm^{-1}: Mo-O_t : 980 cm^{-1},[16,52] Mo-$O_{int(bi)}$: 800-900 cm^{-1} and Mo-O_{Surf} : 700-750 cm^{-1}. As the bridging oxygens are being replaced, several Mo-O, Mo-O-Al, and Al-O-Al peaks start diminishing while peaks of the newly formed Mo-S_t, and Mo-S-Mo appear (around 550 cm^{-1} and below).

Mechanism and kinetics of O/S exchange from Mo_3O_9 to Mo_3S_9 (step I and II)

As explained in detail in Introduction, numerous published experimental works underlined the key role of H_2S during the early stage of sulfo-reduction of Mo-oxide, we will thus assume here that hydrogen will not be involved in the sulfidation mechanisms at the first steps (I and II). Instead, we consider first that O/S exchange by H_2S adsorption and H_2O removal is thermodynamically preferred (as illustrated in what follows), which is in line with the earlier proposal by Muijsers et al.[28] Moreover, using H_2S is also coherent with some experiments that reported MoS_2 formation under pure H_2S environment.[24,26] Note that we preliminary found that the direct reduction of Mo_3O_9 by hydrogen is endothermic (0.2 eV – 1.76 eV for first oxygen removal (**Supporting Information 5.3**) and 0.51 eV – 1.89 eV for the second oxygen removal).

Thus, we will first focus on the role of H_2S and its reactivity on oxides/oxysulfides to trisulfides conversion (in line with steps I and II of **Figure 1**), and further, we will analyze the possible role of H_2 to allow the transformation either from trisulfide to disulfide (**Figure 1**, step IV), or from oxysulfide to disulfide (Figure 1, step-III).

Oxygen to sulfur exchange by H_2S will involve four crucial steps as described in **Scheme 1.**

i)	$* + H_2S(g) \rightarrow *–SH_2$	H_2S adsorption
ii)	$*–O + *–SH_2 \rightarrow *–OH + *–SH$	H_2S dissociation
iii)	$*–OH + *–SH \rightarrow *–OH_2 + *–S$	Proton transfer
iv)	$*–OH_2 \rightarrow * + H_2O_{(g)}$	H_2O desorption
	$*–O + H_2S_{(g)} \rightarrow *–S + H_2O_{(g)}$	

Scheme 1. Main elementary steps for the O/S exchange involving H_2S/H_2O. * represent formally a Mo site of the $Mo_3O_{9-x}S_x$ intermediates (when O_t and O_b are involved), where an O site is removed or where H_2S adsorbs. In some cases, it may also represent an Al site of the (100) γ–alumina surface where H_2S adsorbs (when O_{int} are involved).

Apart from these four main steps, there might be SH or OH reorientation and S migration steps. We have examined the reactivity of all four oxygen sites described before and their respective O/S replacement mechanism steps. According to the previous thermodynamic investigation, bridging/terminal oxygens are the easiest to replace, while interfacial ones are more challenging.

Bridging-oxygen sites. Adsorption and activation of H_2S is the first step towards sulfidation of the starting Mo_3O_9 oxide. Since the targeted replaceable oxygen atoms are the bridging ones, we

restrict the adsorption of H_2S on the Mo central site close to the reactive site. Furthermore, this central Mo-atom was observed to have the strongest capacity to adsorb (confirmed by more exhaustive exploration not reported here) due to its square-pyramidal environment providing one empty site (* in **Scheme 1**) available for H_2S adsorption. While the adsorption energy of H_2S (at 0 K) is exothermic (-0.48 eV, **Figure S15 a**), this step is actually endergonic at 625 K ($\Delta G_{br_{0\to1}} = +0.55$ eV) when including entropy and thermal corrections.

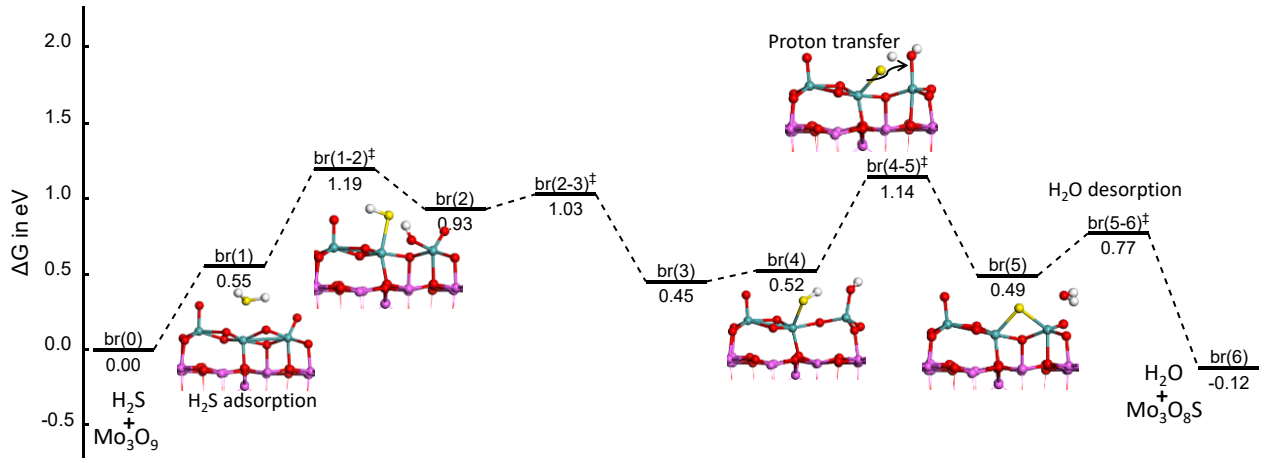

Figure 3. Free energy profile of O/S exchange involving bridging oxygen and H_2S. Color legend: red balls: O, blue balls: Mo, pink balls: Al, yellow balls: S, and white balls: H.

During the next step, the H_2S dissociation with a proton transfer to the targeted oxygen occurs. The activation free energy for this H_2S dissociation is $\Delta G^{\ddagger}_{br_{1\to2}} = +0.64$ eV which is expected to be accessible in sulfo-reductive conditions (T = 625 K). Once H_2S is dissociated, one of its protons is transferred to the bridging oxygen leading to the scission of one Mo-O bond and the simultaneous formation of one OH group. Consequently, the Mo-S bond shortens as H_2S dissociates (from 2.79 Å with H_2S to 2.42 Å with SH), which reveals the strengthening of the interaction of the SH group with the Mo-site with respect to the initial H_2S molecule.

The energy level of the product is quite close to the TS level (br(2) and br(2-3)‡, $\Delta G^{\ddagger}_{br_{2\to3}} = +0.10$ eV) due to their structural similarity. A slight internal arrangement, SH and OH rotations, occurs before the next proton transfer involving weak activation energy around +0.07/0.15 eV (activation for H-rotation not shown here), which is far lower than the barrier of other key steps. Therefore, it is reasonable to neglect these activation steps and assume that they will not significantly impact the overall processes.

After these rearrangements, the proton transfer occurs and is coupled with S migration from top to bridging site and water formation. The S bridging process promotes water formation and desorption by cauterizing the Mo-vacancy site where O is removed. This stabilizing effect also explains why the O/S exchange process is more favored than the direct O-removal by H_2 (**Supplementary Information 5.3**). The free energy of activation of this step is $\Delta G^{\ddagger}_{br_{4\to5}} = +0.62$ eV which is also reasonable. The final step concerns the removal of water which exhibit about free energy of activation of $\Delta G^{\ddagger}_{br_{5\to6}} = +0.28$ eV. The entropy of water makes the overall path slightly exergonic (-0.12 eV).

Top-oxygen sites. According to the thermodynamic study, terminal oxygen would not differ significantly from bridging oxygens. We explored the O/S exchange mechanism for terminal oxygen on a $Mo_3O_7S_2$ oxysulfide where the two bridging atoms have been substituted (**Figure S13**). The same central Mo-site exhibits a slightly weaker molecular adsorption of H_2S with $\Delta G_{t_{0\to1}} = +0.79$ eV in contrast with the previously discussed O/S exchange. With a slight activation free energy barrier of $\Delta G^{\ddagger}_{t_{1\to2}} = +0.18$ eV H_2S dissociates. After subsequent SH/OH rotation (t(2) → t(3)), the proton transfer takes place. This step is also coupled with S migration (from top to bridging site) similarly to the bridging O, which is much less energy-demanding

than the direct creation of O-vacancies on top of the Mo site upon H_2/H_2O exchange (**Supplementary Information 5.3**). The proton transfer associated with S migration is the rate-limiting step for this terminal O/S exchange and is higher ($\Delta G^{\ddagger}_{t_{3\rightarrow4}} = +0.92$ eV) than the rate-limiting step for the bridging O/S one. After water formation, migration of S from bridging site to top site is easily leading to a precursor of the water desorption weakly activated ($\Delta G^{\ddagger}_{t_{5\rightarrow6}} = +0.15$ eV). It must be underlined that the S/O exchange occurring on a top monomeric Mo_1O_3 is located at a lower energy level than the trimeric one (**Supplementary Information 4**).

Interfacial-bidentate oxygen sites. Interfacial oxygens remaining on $Mo_3O_4S_5$ can be considered as top/bridging O-sites are already replaced. $O_{int(bi)}$ interacts with Al through Mo-O-Al linkage. There are two intrinsic complexities for the O/S exchange on these sites: one, O accessibility to H_2S is sterically hindered, and two, strong interaction with Al sites. The adsorption of H_2S on the central Mo-atom is relatively weak compared to the previous cases, and the interfacial oxygen would not be accessible with such pre-adsorbed H_2S on the Mo site. Consequently, we had to consider that H_2S adsorbs on one of the Al sites of support located in the close vicinity of the interfacial oxygen to be exchanged. As support Al sites initiate the mechanism, some intermediate steps might differ from the two previous cases, but the four key steps described in **Scheme 1** remain the same, assuming that one Al site is involved as a free site (*). H_2S is adsorbed on support with a stronger interaction (also involving some H-bonding) than on Mo-site. At 625 K, the H_2S adsorption step is thus slightly less endergonic ($\Delta G_{int-bi_{0\rightarrow1}} = +0.43$ eV, **Figure 4**).

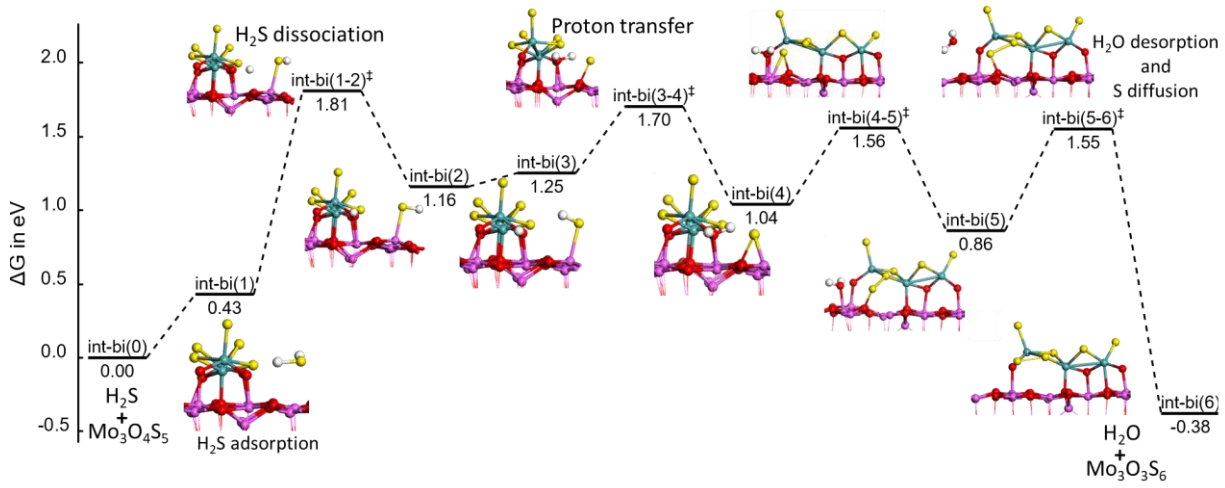

Figure 4. Free energy profile of O/S exchange involving interfacial bidentate oxygen and H_2S. Color legend: red balls: O, blue balls: Mo, pink balls: Al, yellow balls: S, and white balls: H.

H_2S then dissociates by migrating the hydrogen to the replaceable oxygen $O_{int(bi)}$ with an activation energy of $\Delta G^{\ddagger}_{int-bi_{1\to2}} = +1.38$ eV. A relatively large distance between O to be protonated and S during proton transfer(S---H---O) could be the reason for the significantly higher activation free energy than in previous cases. This proton migration also weakens the associated Mo-O bond (2.03 Å vs. 1.81 Å). Furthermore, the instability of SH on the Al site keeps the intermediates at higher energy. This SH group and the subsequent S atom are more stable on the Mo-site of the cluster by 0.54 eV and 0.2 eV, respectively than on Al-site. The next proton transfer step involves a smaller activation energy $\Delta G^{\ddagger}_{int-bi_{3\to4}} = +0.45$ eV (with a high energy level at $+1.70$ eV vs. 1.81 eV for the previous one) and leads to water formation. The H_2O molecule remains bounded to the support's Al site and diffuses on the support before desorbing. In parallel, the S atom formed on the support migrates to the cluster and bonds with a bridging S atom. From a general point of view, the overall mechanism is much more complex than previous ones and involves four high-energy steps (above 1.55 eV).

By contrast, if we consider the monomeric Mo_1OS_2 precursor, S/O exchange occurring on an interfacial bidentate O site of Mo_1OS_2 is located at a significantly lower energy level (+1.35 eV) than the trimeric one (**Supplementary Information 4**). This difference is due to the adsorption of H_2S to the Mo site in the Mo_1OS_2 site (and not on the Al site), which facilitates its activation/dissociation and H-transfer to the interfacial O-site of Mo_1OS_2. This size effect will be further discussed in **Section 4**.

Interfacial-tridentate oxygen site. We consider the MoO_2S_7 oxysulfide intermediate containing one $O_{int(bi)}$ and one $O_{int(tri)}$ site for this step (**Figure S14**). After H_2S adsorption on the support ($\Delta G_{int-tri_{0\rightarrow1}} = +0.37$ eV), the hydrogen atoms of H_2S cannot reach the targeted oxygen site. Hence, H_2S dissociates first on a neighboring alumina μ_3-oxygen and transforms it into μ_2-OH with a weak activation energy of $\Delta G^{\ddagger}_{int-tri_{1\rightarrow2}} = +0.43$ eV. Thereafter, it diffuses and is transferred to the $O_{int(tri)}$ (targeted oxygen) atom forming μ_3-OH with a high activation free energy ($\Delta G^{\ddagger}_{int-tri_{2\rightarrow3}} = +1.00$ eV). Since the proton of SH is too far from $O_{int(tri)}$ to react, the SH group must diffuse from alumina to an accessible terminal sulfide to form a Mo-S-S-H species with a low activation free energy ($\Delta G^{\ddagger}_{int-tri_{4\rightarrow5}} = +0.42$ eV). The proton is more easily accessible to oxygen through this S-S-H species and can be transferred smoothly with a moderate activation free energy of $\Delta G^{\ddagger}_{int-tri_{5\rightarrow6}} = +0.41$ eV. The newly formed water is still in strong interaction with alumina and Mo, which makes the water desorption step demanding with $\Delta G^{\ddagger}_{int-tri_{6\rightarrow7}} = +0.73$ eV, similar to the $O_{int(bi)}$ site. In general, we observe that water desorption from support is kinetically more limited than from a Mo site of the cluster (~0.7 eV vs. ~0.2 eV). The water desorption on Mo-site is promoted by the exchanged S atom, but on the support, it occurs more or less independently. After the

desorption of water, the O-vacancy should be replaced by S, which currently exists as S-S dimer with terminal S. The splitting of the S-S bond requires an activation free energy of $\Delta G^{\ddagger}_{int-tri_{7\rightarrow 8}} = +0.92$ eV. As in the previous case, many energy levels involved are high, and the elementary steps are more numerous, making the overall mechanism much more complex.

3.2 Transformation of Mo_3S_9 trisulfides into Mo_3S_6 disulfides (step IV)

The Mo-trisulfide into disulfide conversion (step IV in **Figure 1)** involves H_2 as a reactant and H_2S as product. The three main elementary steps are described in **Scheme 2**.

i)	2 *–S + H_2 → *–SH + *–SH	H_2 activation
ii)	*–SH + *–SH → *–SH_2 + *–S	Proton transfer
iii)	*–SH_2 → * + H_2S (g)	H_2S desorption
	*–S + H_2 → * + H_2S (g)	

Scheme 2. Main elementary steps for the S removal H_2/H_2S. * represents formally a Mo site of the Mo_3S_{9-x} intermediates. Note: instead of involving 2 Mo-sites, one single site bearing 2 S or one S_2 dimer may be concerned (*–S_2 + H_2 → HS–*–SH_2).

Like in previous cases, some intermediate SH reorientation and S diffusion or rearrangement are also involved. As they are not the limiting ones, we will not report their activation energies. The detailed kinetic pathways corresponding to the different S-species (terminal and bridging) are reported in **Supporting Information 7.2**. One preliminary remark is that we identified possible chain to triangular reconstructions during the Mo_3S_9 to Mo_3S_6 transformation (**Figure 5**). It is known that the targeted MoS_2 phase exhibits a triangular Mo_3 pattern where Mo-atoms

are connected by μ_3-sulfur atoms. Several Mo_3S_9 conformers have been proposed in the literature, such as triangular[21,82,85] or chain-like ones.[78–80,83,86] Hence, one key question for the genesis of the MoS_2 phase could be linked to the kinetics of formation of this triangular pattern. **Figure 5** illustrates the structures of the most relevant Mo_3S_{9-x} intermediates found along the Mo_3S_9 to Mo_3S_6 transformation activated by H_2. As shown in **Figure S18a**, the S-removal steps are almost all isergonic. The chain-like Mo_3S_9 is more stable than triangular-Mo_3S_9 by ~0.5 eV on the alumina support in contrast with their gas-phase structures.[25] As it was already confirmed for the Mo_3O_9 tri-oxide and for $Mo_3O_xS_y$ (x+y = 9) oxysulfides presented before. However, the trend is inverted for the Mo_3S_6 species that are stabilized with a triangular shape due to the undercoordination of Mo in the chain conformer. For 1:3 stoichiometry of Mo:S/O, the interaction with the alumina site is a strong stabilizing factor for the chain conformer over triangular, which involves significant reconstruction of the chain and triangular with respect to their gas-phase ground-state structures. Nevertheless, the support can no longer stabilize chain shapes for Mo:S/O ratio of 1:2 due to the undercoordination of Mo atoms.

Several elementary steps are thus suspected of inducing the chain to the triangular reconstruction of Mo_3S_y intermediates in the course of S removal. This chain to triangular reconstruction may occur at the initial Mo_3S_9 stage (**Figure 5,** bottom path) or while removing sulfur atoms from Mo_3S_9 into Mo_3S_6 (**Figure 5,** top path). The direct Mo_3S_9 chain to triangle reconstruction requires a competing activation free energy of +1.77 eV (**Figure S23**). The complete structural description of this reconstruction is reported in **Supporting Information 8.4.** The triangular-Mo_3S_9 will then further transform into triangular-Mo_3S_6. Even though the triangular-Mo_3S_9 is slightly less stable, the reconstruction may compete with the S-removal on chain conformers involving higher activation energies.

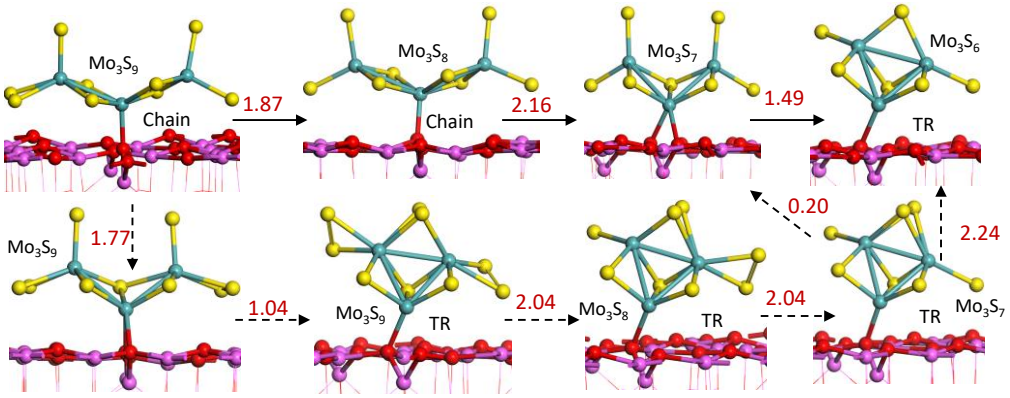

Figure 5. Two possible pathways for the chain-Mo_3S_9 to triangular-Mo_3S_6 transformation: keeping the chain conformation as long as possible (top path), or through triangular-Mo_3S_9 (bottom path). Red numbers are free energies of activation calculated for each given step (referring the highest TS to its lowest energy precursor of the given step, see **Supporting Information 8.1** for the detailed free energy profiles).

To explore how the S-removal occurs, we screened the various possible sites for S removal on-chain and triangular Mo_3S_9 and observed that the terminal-S_2 dimer is kinetically the most prominent to be removed (**Figure S19a** and **S24**). In chain-Mo_3S_9, it leads to a symmetrical structure, and in triangular both terminal-S_2 dimers can be disintegrated likewise. Since the activation free energy of breaking the S_2 dimer along with dissociative adsorption of H_2 is relatively high $\Delta G^{\ddagger}_{Chain_{A_{0\to2}}} = +1.87$ eV (**Figure S19a**) vs. $\Delta G^{\ddagger}_{TR_{t-S2_{0\to2}}} = +2.04$ eV (**Figure S24**), this step would be a rate-limiting step. It is followed by SH rotation, and the third step is a proton transfer from one SH to the neighboring SH leading to the formation of H_2S with activation energy $\Delta G^{\ddagger}_{Chain_{A_{0\to4}}}$ of +1.74 eV. This proton transfer is relatively more accessible for triangular case ($\Delta G^{\ddagger}_{TR_{t-S2\ 0\to4}} = +0.86$ eV). The proton transfer and H_2S desorption are a

concerted process for chain and separate for triangular but with no additional cost. From Mo_3S_9 to Mo_3S_8, the conformation of the cluster remains unchanged.

From Mo_3S_8 to Mo_3S_7, the bridging sulfur is thermodynamically more advantageous than the terminal ones to be removed in the chain conformer. Pulling out, the bridging S creates a vacancy initiating the chain to triangular reconstruction illustrated in **Figure S19b**. As mentioned earlier, the first step would be H_2 dissociation that requires about +1.83 eV ($\Delta G^{\ddagger}_{B_{0\to 2}}$) as activation energy. The proton transfer and the formation of H_2S involves high overall activation energy of $+2.16$ eV ($\Delta G^{\ddagger}_{B_{0\to 4}}$) which asserts to be the rate-limiting step. The desorption of H_2S creates S vacancy and induces the bending of the Mo_3-chain leading to the initiation of a triangular conformer converting bridging sulfur (μ_2-S) into apical sulfur (μ_3-S) with a negligible barrier. The reconstruction results in the stabilization and S-removal process from Mo_3S_8 into Mo_3S_7, which becomes exergonic, contrasting with the previous endergonic S removal. In the case of a triangular conformer, the second S removal from terminal-S_2 dimer is assumed to occur in a similar fashion as the first one.

The remaining excessive sulfur of Mo_3S_7 is removed identically (**Figure 6**) with a rate-limiting step of proton transfer ($\Delta G^{\ddagger}_{C_{0\to 4}} = 1.49$ eV). As in the previous case, the H_2S removal is associated with a further reconstruction, and terminal μ_1-S converted into bridging μ_2-S, which closes the triangular pattern of the Mo_3S_6 disulfide. This structure is reminiscent of the triangular pattern observed in MoS_2 phases. In the triangular case, the bridging S_2-dimer dissociates and converts into the triangular Mo_3S_7 observed from the chain conformer, and S-excess is removed in the same way (**Figure 5**).

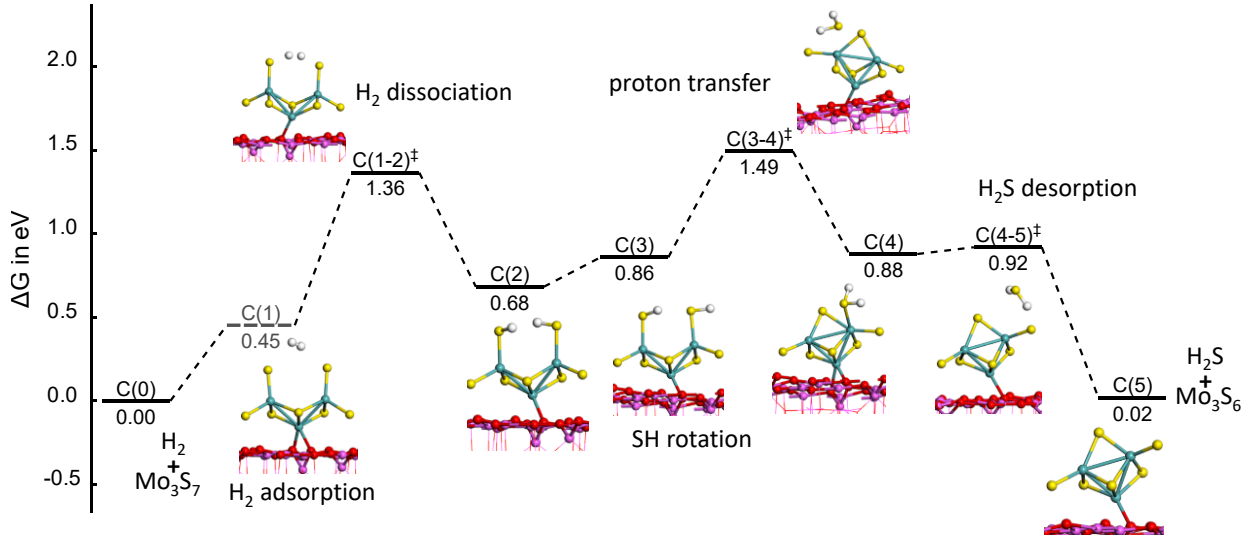

Figure 6. Free energy profile of S removal using H_2 and formation of the triangular Mo_3 pattern: $Mo_3S_7 + H_2 \rightarrow Mo_3S_6 + H_2S$. C(1) corresponding to H_2 physisorbed precursor state is subject to higher uncertainty on its entropic contribution so its free energy level is represented with a dashed line. Color legend: red balls: O, blue balls: Mo, pink balls: Al, yellow balls: S, and white balls: H.

It could be noticed that the various calculated free energies for H_2 activation through homolytic dissociation leading to two Mo-SH groups on Mo_3S_x trimer, such as reported in **Figure 6** or in **Supplementary Information 7.2** are very consistent with those previously found on MoS_2 edges.[87] Even if we cannot fully rule out that this activation step might occur through a heterolytic dissociation (Mo-H and Mo-SH) such as found on monomeric Mo_1S_3 (**Figure S31**), the calculated values reported in Ref.[87] indicate that the heterolytic dissociations are in the same range of the homolytic ones. Hence, the trend reported in our work might not be strongly affected.

3.3 Transformation of $Mo_3O_3S_6$ oxysulfides into Mo_3S_6 disulfides (step III)

As explained in the Introduction, Mo_3S_6 formation may occur through the direct reduction of $Mo_3O_3S_6$ by H_2 (so-called oxysulfide pathway: step III in **Figure 1**) without further use of H_2S. The mechanism involves O-removal and water as a product, and it can be written in a similar way as in **Scheme 2**). After every O removal step, cluster reconstruction occurs and eventually leads to the formation of TR-Mo_3S_6, whereas the initial state of $Mo_3O_3S_6$ oxysulfide is chain-like. Activation energies are comparable to those involved in the trisulfide pathway except for the last O-removal, which is highly unfavored. For the sake of clarity, the detailed results are reported in **Supporting Information 7.3** and discussed in the next section.

4. Discussion

4.1. O/S exchanges from Mo_3O_9 to $Mo_3O_3S_6$ (step I)

Considering Step I of **Figure 1**, our study confirms that the sulfidation of highly dispersed Mo-oxide oligomers involves an O/S exchange mechanism, as previously proposed in the literature.[16,24,28] This mechanism involves four successive elementary steps: i) adsorption of H_2S on Mo site, ii) dissociation of H_2S by migrating the proton to neighboring O, iii) proton transfer from SH to OH resulting in water formation, and d) water desorption. Simultaneously, we identify the nature of oxy-sulfide species and quantify their interaction with alumina support from thermodynamic and kinetic aspects. Though the thermodynamic energy favors the $O_{int(bi)}$ replacement to form S-S dimer according to a heterogenous path, these oxygens involve the highest activation energies, which might kinetically prohibit the sulfidation of these oxygens before bridging or terminal ones. Similarly, $O_{int(tri)}$ would be one of the last oxygens to be replaced due their even lower accessibility.

If we consider the thermodynamic diagram (homogeneous path-1 vs. heterogeneous path-2 in **Figure 2**), O/S exchange will follow path-1 at the early stage of sulfidation since bridging and terminal oxygens are easily replaceable kinetically. Some earlier DFT studies on unsupported bulk MoO_3 found that the top oxo species are thermodynamically preferred,[44–46] which difference can be explained by the distorted Mo_3O_9 chain structure which enhance the reactivity of bridging oxo site. Once the second interfacial oxygen is replaced ($Mo_3O_3S_6 \rightarrow Mo_3O_2S_7$), a transition from the homogeneous path-1 to the heterogenous path-2 should occur. If heterogeneous path-2 occurs preferentially, the oxysulfide intermediate such as $Mo_3O_3S_6$ will retain the oxo (terminal) species for a longer sulfidation degree, which is compatible with EXAFS observations showing the presence of the smallest Mo-O bonds also for $Mo_3O_3S_6$.[17,18]

4.2. Competition between oxysulfide pathway and trisulfide pathway

The summarized free energy profile shown in **Figure 7,** is based on the dominating kinetics showing that the O/S exchange occurs in the following order: $O_{br} > O_t > O_{int\text{-}bi} > O_{int\text{-}tri}$. Based on several tests, we assume that the same types of oxygen (or sulfur) sites exhibit similar kinetic barriers (although some of them have not been calculated explicitly). We compare in what follows the free energies of activation of the Rate Determining Transition States (RDTS) and Determining Intermediates (RDI) and propose an overall discussion on kinetic effects.

In **Figure 7,** until the formation of $Mo_3O_3S_6$, the rate-limiting step is exchanging the $O_{int\text{-}bi}$ ($\Delta G^{\ddagger}_{int-bi}$= 1.81 eV). The next O/S exchange is competing with O removal by a direct reduction pathway (steps III in **Figure 1**): from Mo-oxysulfide ($Mo_3O_3S_6$), removing interfacial oxygen with H_2 requires comparable free activation energies as replacing the same oxygen sites by S

(+1.85 eV vs. +1.79 eV). Moreover, thermodynamically the O/S exchange also competes with reduction accompanied by oxygen removal. Indeed, the RDI of the trisulfide pathway obtained for the Mo_3OS_8 intermediate, exhibits a very similar free energy (~ -2 eV) as for the RDI Mo_3OS_6 in the O-removal of the oxysulfide path. Therefore, it seems challenging to discriminate between O/S exchange leading to Mo_3OS_8 (step II) and oxygen removal (step III) leading to Mo_3OS_6 starting from the common $Mo_3O_3S_6$ intermediate. Exchanging the final oxygen by sulfur ($Mo_3OS_8 \rightarrow Mo_3S_9$) is endergonic ($\Delta G$=+0.32 eV) and requires the maximum activation energy among all O/S exchanges ($\Delta G^{\ddagger}_{int-tri}$ = +1.93 eV). By contrast, the last O-removal on Mo_3OS_6 reveals a kinetic limitation due to the high-energy intermediate generated (+2.68 eV of Mo_3S_6) before its reconstruction towards the most stable one. Instead of removing the last oxygen in Mo_3OS_6 alternatively, it can be replaced by the O/S exchange leading to Mo_3S_7. This alternative step reveals a free activation energy of $\Delta G^{\ddagger}_{F(4-5)}$ +1.96 eV (**Figure S21c**), which is the highest value among all the individual activation energies found for the mechanisms studied in this work. After replacing this O with S, it will transform into Mo_3S_7, and the last S removal step, to eventually transform into Mo_3S_6, will be the same as the trisulfide path (**Figure 6**). Considering the limitation for the last interfacial oxygen removal, the trisulfide pathway involving Mo_3S_9 seems to be more favorable than the direct reduction from $Mo_3O_3S_6$ (oxysulfide) to Mo_3S_6 (disulfide). Nonetheless, Mo_3S_9 eventually has also to transform into disulfide Mo_3S_6.

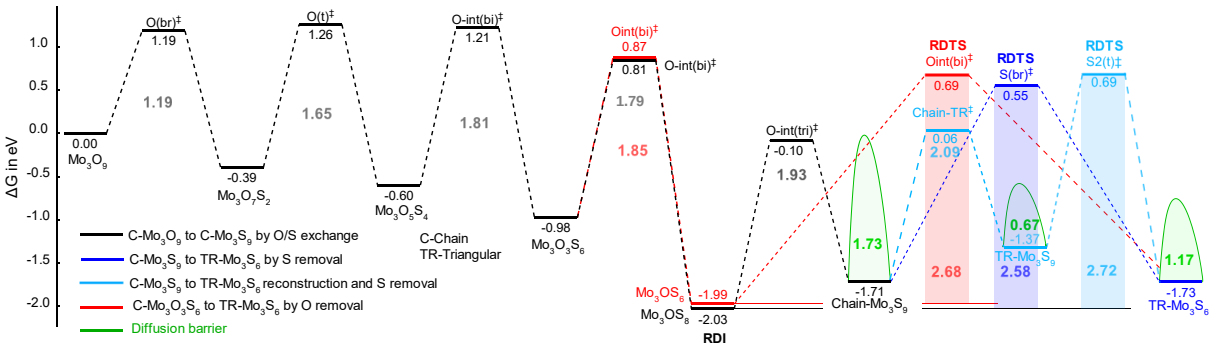

Figure 7. Free energy comparison of entire sulfo-reduction pathways from chain-Mo_3O_9 to TR-Mo_3S_6 formation: O/S exchange (black: step III), chain to triangular reconstruction and S-removal to disulfide (light blue: step-III), chain-trisulfide to triangular disulfide by S-removal (dark blue: step-III) and oxysulfide to disulfide by O-removal (red: step IV) with respective rate-limiting step and involved oxygen or sulfur species. The corresponding RDI and RDTS are also mentioned for the concerned pathways. The green curve shows the barrier for translatory diffusion of sulfide on (100) surfaces of γ-alumina. The entire energy profile is reported in **Figure S30**.

Regarding the transformation of chain Mo_3S_9 into triangular Mo_3S_6, the sulfur removal steps are clearly kinetically unfavored since relatively high free activation energies are required for the S-removals (+2.58 eV with respect to RDI, **Figure 7**). Hence, after the formation of chain-Mo_3S_9, we must consider an alternate path where the reconstruction to a triangular conformer may take place before S-removal on chain Mo_3S_9. The exploration of this alternate path (**Supporting Information 8.1)** is also justified by the fact that the trisulfide Mo_3S_9 phase has a much weaker interaction with the support than all other chain-like oxysulfide intermediates (see also next section), suggesting that this transformation should be more accessible at the trisulfide stage than at the oxysulfide stage. The activation energy of this Mo_3S_9 chain to triangle

reconstruction is about +2.09 eV (related to RDI, **Figure 7**) which is preferred to the direct formation of Mo_3S_6 intermediate through S- or O-removal. However, the subsequent removals of S-atoms from TR-Mo_3S_9 to TR-Mo_3S_6 are again kinetically limited (+2.72 eV, **Figure S24** and **Figure 7**). Chain and triangular Mo_3S_9 are thus kinetically accessible, but the subsequent steps of S-removals are kinetically prohibited. So, the unique alternative for the Mo_3S_9 intermediates to evolve could be to diffuse on the alumina surface and grow before giving rise to the MoS_2 phase as discussed in the following.

4.3. Mobility, growth, and size effects

As quantified in **Supporting Information 9.1,** the interaction energy of Mo-oxysulfides and Mo-sulfides with alumina reveals that the Mo-sulfides oligomers are the less strongly bonded species, as expected from chemical intuition. Based on this preliminary interaction energy analysis, we have quantified the translational diffusion of 4 key Mo-sulfide species (chain-Mo_3S_9, triangular-Mo_3S_9 and triangular-Mo_3S_6, and Mo_1S_3) on the alumina (100) surface following some main principal orientations of the surface, which allow the migration of the oligomers from one O site to another (**Supporting Information 9.2**). The translational diffusion barrier is significantly higher for chain-Mo_3S_9 than for triangular conformers (1.73 eV vs. 0.67 eV). Therefore, the mobility of Mo_3S_9 triangular intermediates is favored with respect to chain-Mo_3S_9. We thus expect that the growth of MoS_3-polymorphs should be predominant through Mo_3S_9 triangular species before their ultimate transformation into the MoS_2 active phase, as suggested by the observed sizes of sulfides evaluated by EXAFS studies.[8,17,18] The diffusion

barrier of triangular-Mo_3S_9 is also lower than Mo_3S_6 (0.67 eV vs. 1.17 eV). Therefore, if Mo_3S_6 species are formed, their mobility could also allow the formation of the MoS_2 phase. Since the S-removals on chain-Mo_3S_9 are kinetically limited as aforementioned, the chain to triangle reconstruction followed by diffusion of triangular-Mo_3S_9 will preferentially occur. This diffusion process will allow their subsequent condensation into larger trisulfide $Mo_{3n}S_{9n}$ 2D patches of finite size, so called 1T'-MoS_3 phase in our previous study.[25] Molecular dynamics simulation revealed that the condensation of triangular-$(Mo_3S_9)_{n\ (n=2,3)}$ oligomers into $Mo_{3n}S_{9n}$ 2D patches is indeed possible in gas phase.[25] Moreover, According to Ref.[25], the energy gain by the condensation of isolated triangular-Mo_3S_9 into $Mo_{3n}S_{9n}$ 2D patches is substantial (around -2 eV to -2.5 eV/Mo_3S_9 depending on n). Since the interaction energy of triangular-Mo_3S_9 on γ–alumina is about -1.5 eV (**Figure S25**), this implies that the formation of such 2D patches from triangular-Mo_3S_9 dispersed on alumina is an exothermic process. If so, the S-removal steps would occur on such larger size $Mo_{3n}S_{9n}$ 2D patches rather than on the Mo_3S_9 for which the S-removal is energetically too demanding. **Supporting Information SI.11** and **Figure 8** show that the estimated barriers for the S-removal step decrease by increasing the Mo trisulfides cluster size. This S-removal results in the transformation of $Mo_{3n}S_{9n}$ 2D patches into $Mo_{3n}S_{6n}$ 2D patches which could diffuse and futher grow to form the crystalline MoS_2 phase.

We also expect that even smaller Mo trisulfides entities (Mo_2S_6 or Mo_1S_3, **Figure S29**) diffuse easily to enable the growth of the MoS_3 phase. Such fast diffusing trisulfide surface monomers, dimers or trimers might be at the origin of the layer-by-layer growing process of the MoS_2 phase supported on $MgAl_2O_4$ observed by in situ TEM.[30]

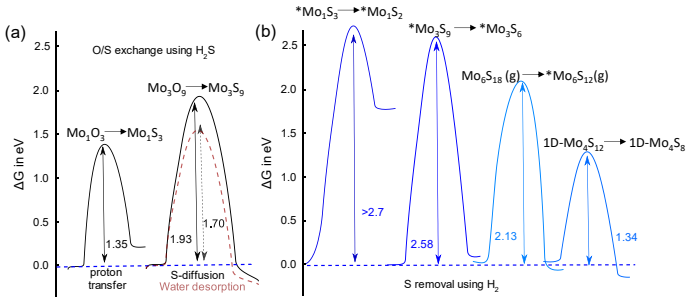

Figure 8. Comparison of Gibbs free energies of activation for O/S exchange and S-removal for diverse sizes. * denotes the supported species, g: gas phase, and 1D: 1 dimensional periodic.

Moreover, the O/S exchange step is also influenced by the effect of size, and the monomeric Mo_1O_3 cluster exhibits a significantly smaller activation free energy of +1.35 eV (**Supporting Information SI.4**) than Mo_3O_9. This implies that the trisulfide pathway (steps I and II in **Figure 1**) should be predominant for small MoO_3 oligomers, including monomeric ones. Therefore, once these small Mo oxide clusters are trisulfided, they rapidly diffuse on the alumina surface (**Figure S29**) and grow to form larger $Mo_{3n}S_{9n}$ 2D patches before transforming into MoS_2 phase by S-removals.

5. Conclusions

Using DFT calculations, we examined the sulfo-reduction mechanisms of Mo-oxide oligomers on the (100) surface of γ-alumina support. Mo-oxysulfides model intermediates have been validated by comparison with available structural data and IR spectra. As first perspective, we propose that the numerous Mo-oxysulfide structures identified in this work could be used for the simulation of in situ X-ray Absorption Spectra (EXAFS or XANES) in order to help for a refined identification of the key intermediates involved in the sulfo-reduction pathway.

We compared the two competing pathways of the genesis of the active phase: the first one involving Mo-oxysulfide intermediate only and the second one involving Mo-oxysulfide/Mo-trisulfide. A complete free energy analysis has been performed, accounting for various effects: the oligomer size, the chain to triangular shape reconstruction, and the diffusion of the Mo clusters on the alumina surface. Based on the gained understanding, we propose a comprehensive reaction network for the sulfidation/reduction process from Mo_3O_9 oxide to MoS_3 and MoS_2 active phase, as summarized in **Figure 9**.

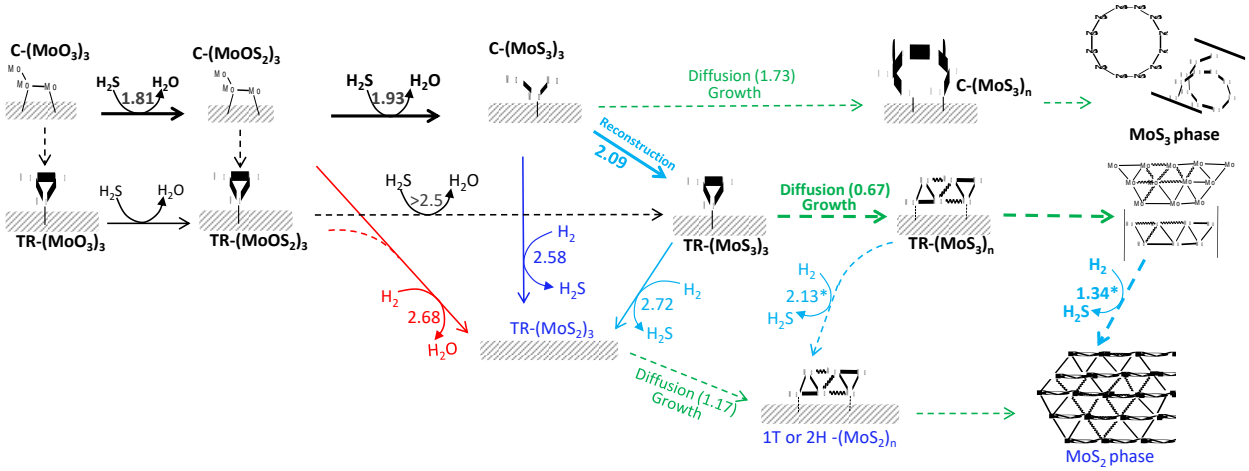

Figure 9. Schematic representation of the entire reaction network during activation, starting from Mo-oxide precursors to final MoS_2 active phase. (C-Chain; TR-Triangular, * values are estimated on unsupported clusters and periodic structures)

As shown in **Figure 9**, a sulfo-reduction pathway of Mo-oxides on alumina (100) surface, leading to the MoS_2 phases, should proceed as follows.

- The sulfidation of Mo_nO_{3n} into Mo_nS_{3n} becomes progressively harder from x=1 to x=3 and occurs via a S/O exchange mechanism (dark arrows in **Figure 9**), whereas the O-removal is extremely demanding (red arrows). The kinetic order of O/S exchange in Mo_3O_9 follows: $O_{br} > O_t > O_{int\text{-}bi} > O_{int\text{-}tri}$.

- The chain-like Mo_3S_9 cluster should reconstruct into a triangular one to be able to transform further (plain light blue arrows in **Figure 9**).
- The small size Mo_nS_{3n} oligomers ($x \leq 3$, including triangular Mo_3S_9) are fast diffusing species and oligomerize into larger species (dashed green arrows in **Figure 9**), last but not least into $(Mo_3S_9)_n$ 2D patches.
- For Mo_3S_9, the S-removal occurs preferentially on terminal-S_2 and terminal-S while bridging S requires the highest activation energy. However, the S-removal is expected to take place at a lower cost on larger $(Mo_3S_9)_n$ 2D patches (dashed blue arrows in **Figure 9**).
- As discussed in Ref.,[25] these $(Mo_3S_9)_n$ 2D patches may be the precursor of the 1T-MoS_2 phase, subsequently leading to 2H-MoS_2.

Since we analyzed the role of H_2S and H_2 as individual reactant leading to sulfidation and/or reduction, we propose as a second perspective to investigate if an interplay could exist between both reactants being simultaneously involved in the elementary steps.

We found that the support shows a substantial impact on energetics and structures (with respect to isolated species): cyclic-Mo_3O_9 and triangular Mo_3S_9 are more stable in the gas phase, while the alumina (100) surface stabilizes the linear conformers through single or multiple Mo-O-Al bonds. Nevertheless, we expect that the specific alumina facet may impact the mobility of the species that we have quantified in the present work. In the future, it would thus be relevant to extend the study to other γ-alumina surfaces which were proposed to influence the sulfidation

degree of the MoS_2 phase,[48,49] and which features OH groups under sulfo-reduction conditions together with other Al sites as compared to the (100) surface.

Supporting Information. The gas phase sulfidation, and complementary data on thermodynamics, kinetics and frequency analyses of various pathways (including diffusion and reconstruction) for monomers and trimers, EXAFS and IR comparison for intermediates, have been reported in supporting information. The structural data for all intermediates and transition states are available from the corresponding author upon reasonable request. [32]

Funding Sources

Calculations were performed using HPC resources (Jean Zay and Occigen) from GENCI-CINES (Grant A0020806134) and ENER 440 from IFP Energies nouvelles. This work is part of the "RatiOnAl Design for CATalysis" (ROAD4CAT) industrial chair, project IDEXLYON funded by the French National Research Agency (ANR-16-IDEX-0005) and the Commissariat-General for Investment (CGI) within the framework of Investissements d'Avenir program ("Investment for the future"). The authors thank the SYSPROD project and AXELERA Pôle de Compétitivité for financial support (PSMN Data Center).

Acknowledgements

The authors acknowledge C. Legens from IFP Energies Nouvelles for fruitful discussions on EXAFS experimental data.

References

[1] H. Toulhoat, P. Raybaud, Catalysis by transition metal sulphides: From molecular theory to industrial application, Editions Technip, Paris, France, 2013.

[2] P. Euzen, P. Raybaud, X. Krokidis, H. Toulhoat, J.-L. Le Loarer, J.-P. Jolivet, C. Froidefond, Alumina, in: Schüth, Sing et al. (Ed.) 2002 – Handbook of Porous Solids, pp. 1591–1677.

[3] M. Breysse, P. Afanasiev, C. Geantet, M. Vrinat, Overview of support effects in hydrotreating catalysts, Catal. Today 86 (2003) 5–16.

[4] M. Breysse, C. Geantet, P. Afanasiev, J. Blanchard, M. Vrinat, Recent studies on the preparation, activation and design of active phases and supports of hydrotreating catalysts, Catal. Today 130 (2008) 3–13.

[5] J. Ramirez, S. Fuentes, G. Díaz, M. Vrinat, M. Breysse, M. Lacroix, Hydrodesulphurization activity and characterization of sulphided molybdenum and cobalt—molybdenum catalysts comparison of alumina-, silica—alumina- and titania-supported catalysts, Appl. Catal. 52 (1989) 211–223.

[6] R. Huirache-Acuña, R. Nava, C.L. Peza-Ledesma, J. Lara-Romero, G. Alonso-Núez, B. Pawelec, E.M. Rivera-Muñoz, SBA-15 Mesoporous Silica as Catalytic Support for Hydrodesulfurization Catalysts—Review, Materials 6 (2013) 4139–4167.

[7] S. Texier, G. Berhault, G. Pérot, F. Diehl, Activation of alumina-supported hydrotreating catalysts by organosulfides or H_2S: Effect of the H_2S partial pressure used during the activation process, Appl. Catal. A 293 (2005) 105–119.

[8] C. Lesage, E. Devers, C. Legens, G. Fernandes, O. Roudenko, V. Briois, High pressure cell for edge jumping X-ray absorption spectroscopy: Applications to industrial liquid sulfidation of hydrotreatment catalysts, Catal. Today 336 (2019) 63–73.

[9] Y. Jacquin, J.P. Franck, G. Goubin, A. Elchenberger, 06/19/1985 Patent EP 0064429 B2.

[10] S. Eijsbouts, L.C.A. van den Oetelaar, J.N. Louwen, R.R. van Puijenbroek, G.C. van Leerdam, Changes of MoS_2 Morphology and the Degree of Co Segregation during the Sulfidation and Deactivation of Commercial Co−Mo/Al_2O_3 Hydroprocessing Catalysts, Ind. Eng. Chem. Res. 46 (2007) 3945–3954.

[11] N. Frizi, P. Blanchard, E. Payen, P. Baranek, C. Lancelot, M. Rebeilleau, C. Dupuy, J.P. Dath, Genesis of new gas oil HDS catalysts: Study of their liquid phase sulfidation, Catal. Today 130 (2008) 32–40.

[12] L. van Haandel, G.M. Bremmer, E. Hensen, T. Weber, Influence of sulfiding agent and pressure on structure and performance of CoMo/Al_2O_3 hydrodesulfurization catalysts, J. Catal. 342 (2016) 27–39.

[13] C.H. Chang, S.S. Chan, Infrared and Raman studies of amorphous MoS_3 and poorly crystalline MoS_2, J. Catal. 72 (1981) 139–148.

[14] S.P. Cramer, K.S. Liang, A.J. Jacobson, C.H. Chang, R.R. Chianelli, EXAFS studies of amorphous molybdenum and tungsten trisulfides and triselenides, Inorg. Chem. 23 (1984) 1215–1221.

[15] R. Cattaneo, T. Weber, T. Shido, R. Prins, A Quick EXAFS Study of the Sulfidation of NiMo/SiO_2 Hydrotreating Catalysts Prepared with Chelating Ligands, J. Catal. 191 (2000) 225–236.

[16] T. Weber, J.C. Muijsers, J.H.M.C. van Wolput, C.P.J. Verhagen, J.W. Niemantsverdriet, Basic Reaction Steps in the Sulfidation of Crystalline MoO_3 to MoS_2, As Studied by X-ray Photoelectron and Infrared Emission Spectroscopy, J. Phys. Chem. 100 (1996) 14144–14150.

[17] A. Rochet, B. Baubet, V. Moizan, C. Pichon, V. Briois, Co-K and Mo-K edges Quick-XAS study of the sulphidation properties of Mo/Al_2O_3 and CoMo/Al_2O_3 catalysts, C. R. Chim. 19 (2016) 1337–1351.

[18] A. Rochet, B. Baubet, V. Moizan, E. Devers, A. Hugon, C. Pichon, E. Payen, V. Briois, Intermediate Species Revealed during Sulfidation of Bimetallic Hydrotreating Catalyst, J. Phys. Chem. C 121 (2017) 18544–18556.
[19] R.G. Leliveld, A.J. van Dillen, J.W. Geus, D.C. Koningsberger, The Sulfidation of γ-Alumina and Titania Supported (Cobalt)Molybdenum Oxide Catalysts Monitored by EXAFS, J. Catal. 171 (1997) 115–129.
[20] P. Arnoldy, J. van den Heijkant, G.D. de Bok, J.A. Moulijn, Temperature-programmed sulfiding of MoO_3/Al_2O_3 catalysts, J. Catal. 92 (1985) 35–55.
[21] T. Weber, J.C. Muijsers, J.W. Niemantsverdriet, Structure of Amorphous MoS_3, J. Phys. Chem. 99 (1995) 9194–9200.
[22] R. Cattaneo, F. Rota, R. Prins, An XAFS Study of the Different Influence of Chelating Ligands on the HDN and HDS of γ-Al_2O_3-Supported NiMo Catalysts, J. Catal. 199 (2001) 318–327.
[23] D. Nicosia, R. Prins, The effect of phosphate and glycol on the sulfidation mechanism of $CoMo/Al_2O_3$ hydrotreating catalysts, J. Catal. 231 (2005) 259–268.
[24] E. Payen, S. Kasztelan, S. Houssenbay, R. Szymanski, J. Grimblot, Genesis and characterization by laser Raman spectroscopy and high-resolution electron microscopy of supported molybdenum disulfide crystallites, J. Phys. Chem. 93 (1989) 6501–6506.
[25] A. Sahu, S.N. Steinmann, P. Raybaud, Size-Dependent Structural, Energetic, and Spectroscopic Properties of MoS_3 Polymorphs, Crystal Growth & Design 20 (2020) 7750–7760.
[26] B. Baubet, M. Girleanu, A.-S. Gay, A.-L. Taleb, M. Moreaud, F. Wahl, V. Delattre, E. Devers, A. Hugon, O. Ersen, P. Afanasiev, P. Raybaud, Quantitative Two-Dimensional (2D) Morphology–Selectivity Relationship of CoMoS Nanolayers: A Combined High-Resolution High-Angle Annular Dark Field Scanning Transmission Electron Microscopy (HR HAADF-STEM) and Density Functional Theory (DFT) Study, ACS Catal. 6 (2016) 1081–1092.
[27] B. Scheffer, E.M. van Oers, P. Arnoldy, V. de Beer, J.A. Moulijn, Sulfidability and HDS activity of Co-Mo/Al_2O_3 catalysts, Appl. Catal. 25 (1986) 303–311.
[28] J.C. Muijsers, T. Weber, R.M. Vanhardeveld, H.W. Zandbergen, J.W. Niemantsverdriet, Sulfidation Study of Molybdenum Oxide Using $MoO_3/SiO_2/Si(100)$ Model Catalysts and Mo_3^{IV}-Sulfur Cluster Compounds, J. Catal. 157 (1995) 698–705.
[29] A. Rochet, B. Baubet, V. Moizan, E. Devers, A. Hugon, C. Pichon, E. Payen, V. Briois, Influence of the Preparation Conditions of Oxidic $NiMo/Al_2O_3$ Catalysts on the Sulfidation Ability: A Quick-XAS and Raman Spectroscopic Study, J. Phys. Chem. C 119 (2015) 23928–23942.
[30] L.P. Hansen, E. Johnson, M. Brorson, S. Helveg, Growth Mechanism for Single- and Multi-Layer MoS_2 Nanocrystals, J. Phys. Chem. C 118 (2014) 22768–22773.
[31] J. Handzlik, P. Sautet, Structure of Isolated Molybdenum(VI) Oxide Species on γ-Alumina: A Periodic Density Functional Theory Study, J. Phys. Chem. C 112 (2008) 14456–14463.
[32] J. Handzlik, P. Sautet, Structure of Dimeric Molybdenum(VI) Oxide Species on γ-Alumina: A Periodic Density Functional Theory Study, J. Phys. Chem. C 114 (2010) 19406–19414.
[33] K. Hamraoui, S. Cristol, E. Payen, J.-F. Paul, Computational Investigation of TiO_2-Supported Isolated Oxomolybdenum Species, J. Phys. Chem. C 111 (2007) 3963–3972.
[34] K. Hamraoui, S. Cristol, E. Payen, J.-F. Paul, Structure and reducibility of titania-supported monomeric and dimeric molybdenum oxide entities studied by DFT calculations, J. Mol. Struct. THEOCHEM 903 (2009) 73–82.
[35] A. Tougerti, E. Berrier, A.-S. Mamede, C. La Fontaine, V. Briois, Y. Joly, E. Payen, J.-F. Paul, S. Cristol, Synergy between XANES Spectroscopy and DFT to Elucidate the Amorphous Structure of Heterogeneous Catalysts: TiO_2-Supported Molybdenum Oxide Catalysts, Angew. Chem. Int. Ed. 52 (2013) 6440–6444.

[36] H. Hu, D. Oliveira de Souza, E. Berrier, J.-F. Paul, C. La Fontaine, V. Briois, S. Cristol, A. Tougerti, Investigation of the Reducibility of Supported Oxomolybdate Species for Mapping of Active Centers of Partial Oxidation Reaction: In Situ Mo K-Edge XAS and DFT Study, J. Phys. Chem. C 123 (2019) 18325–18335.
[37] D. Kiani, S. Sourav, W. Taifan, M. Calatayud, F. Tielens, I.E. Wachs, J. Baltrusaitis, Existence and Properties of Isolated Catalytic Sites on the Surface of β-Cristobalite-Supported, Doped Tungsten Oxide Catalysts (WO_x/β-SiO_2, Na-WO_x/β-SiO_2, Mn-WO_x/β-SiO_2) for Oxidative Coupling of Methane (OCM): A Combined Periodic DFT and Experimental Study, ACS Catal. 10 (2020) 4580–4592.
[38] C. Arrouvel, M. Breysse, H. Toulhoat, P. Raybaud, A density functional theory comparison of anatase (TiO_2)- and γ-Al_2O_3-supported MoS_2 catalysts, J. Catal. 232 (2005) 161–178.
[39] D. Costa, C. Arrouvel, M. Breysse, H. Toulhoat, P. Raybaud, Edge wetting effects of γ-Al_2O_3 and anatase-TiO_2 supports by MoS_2 and CoMoS active phases, J. Catal. 246 (2007) 325–343.
[40] B. Hinnemann, J.K. Nørskov, H. Topsøe, A Density Functional Study of the Chemical Differences between Type I and Type II MoS_2-Based Structures in Hydrotreating Catalysts, J. Phys. Chem. B 109 (2005) 2245–2253.
[41] N. Abidi, A. Bonduelle-Skrzypczak, S.N. Steinmann, How Stable Are 2H-MoS2 Edges under Hydrogen Evolution Reaction Conditions?, J. Phys. Chem. C 125 (2021) 17058–17067.
[42] M. Yu, W. Qu, S. Xu, L. Wang, B. Liu, L. Zhang, J. Peng, Interfacial stability, electronic property, and surface reactivity of α-MoO_3/γ-Al_2O_3 composites, Comput. Mater. Sci. 153 (2018) 217–227.
[43] M. Shahrokhi, P. Raybaud, T. Le Bahers, On the understanding of the optoelectronic properties of S-doped MoO_3 and O-doped MoS_2 bulk systems: a DFT perspective, J. Mater. Chem. C 8 (2020) 9064–9074.
[44] S. Hong, S. Tiwari, A. Krishnamoorthy, K. Nomura, C. Sheng, R.K. Kalia, A. Nakano, F. Shimojo, P. Vashishta, Sulfurization of MoO_3 in the Chemical Vapor Deposition Synthesis of MoS_2 Enhanced by an H_2S/H_2 Mixture, J. Phys. Chem. Lett. 12 (2021) 1997–2003.
[45] X.-R. Shi, J. Wang, K. Hermann, Theoretical Cluster Studies on the Catalytic Sulfidation of MoO_3, J. Phys. Chem. C 114 (2010) 6791–6801.
[46] M. Misawa, S. Tiwari, S. Hong, A. Krishnamoorthy, F. Shimojo, R.K. Kalia, A. Nakano, P. Vashishta, Reactivity of Sulfur Molecules on MoO_3 (010) Surface, J. Phys. Chem. Lett. 8 (2017) 6206–6210.
[47] Y.V. Joshi, P. Ghosh, M. Daage, W.N. Delgass, Support effects in HDS catalysts, J. Catal. 257 (2008) 71–80.
[48] C. Bara, L. Plais, K. Larmier, E. Devers, M. Digne, A.-F. Lamic-Humblot, G.D. Pirngruber, X. Carrier, Aqueous-Phase Preparation of Model HDS Catalysts on Planar Alumina Substrates: Support Effect on Mo Adsorption and Sulfidation, J. Am. Chem. Soc. 137 (2015) 15915–15928.
[49] R. Garcia de Castro, J. Bertrand, B. Rigaud, E. Devers, M. Digne, A.-F. Lamic-Humblot, G. Pirngruber, X. Carrier, Surface-Dependent Activation of Model α-Al2O3-Supported P-Doped Hydrotreating Catalysts Prepared by Spin Coating, Chem. Eur. J. 26 (2020) 14623–14638.
[50] J. Handzlik, P. Sautet, Active sites of olefin metathesis on molybdena-alumina system, J. Catal. 256 (2008) 1–14.
[51] N. Ohler, A.T. Bell, Study of the Elementary Processes Involved in the Selective Oxidation of Methane over MoO_x/SiO_2, J. Phys. Chem. B 110 (2006) 2700–2709.
[52] J.L.G. Fierro, Metal Oxides: Chemistry and applications, CRC PRESS, 2006.
[53] J.M. Stencel, L.E. Makovsky, T.A. Sarkus, J. de Vries, R. Thomas, J.A. Moulijn, Raman spectroscopic investigation of the effect of H_2O on the molybdenum surface species in MoO_3-Al_2O_3 catalysts, J. Catal. 90 (1984) 314–322.
[54] H. Hu, I.E. Wachs, S.R. Bare, Surface Structures of Supported Molybdenum Oxide Catalysts, J. Phys. Chem. 99 (1995) 10897–10910.

[55] G. Xiong, C. Li, Z. Feng, P. Ying, Q. Xin, J. Liu, Surface Coordination Structure of Molybdate with Extremely Low Loading on γ-Alumina Characterized by UV Resonance Raman Spectroscopy, J. Catal. 186 (1999) 234–237.
[56] A.N. Desikan, L. Huang, S.T. Oyama, Structure and dispersion of molybdenum oxide supported on alumina and titania, J. Chem. Soc., Faraday Trans. 88 (1992) 3357–3365.
[57] G. Mestl, T.K.K. Srinivasan, Raman Spectroscopy of Monolayer-Type Catalysts, Catal. Rev. 40 (1998) 451–570.
[58] G. Kresse, J. Hafner, Ab initio molecular dynamics for liquid metals, Phys. Rev. B 47 (1993) 558–561.
[59] G. Kresse, J. Furthmüller, Efficient iterative schemes for ab initio total-energy calculations using a plane-wave basis set, Phys. Rev. B 54 (1996) 11169–11186.
[60] G. Kresse, J. Furthmüller, Efficiency of ab-initio total energy calculations for metals and semiconductors using a plane-wave basis set, Comput. Mater. Sci. 6 (1996) 15–50.
[61] J.P. Perdew, K. Burke, M. Ernzerhof, Generalized Gradient Approximation Made Simple, Phys. Rev. Lett. 77 (1996) 3865–3868.
[62] S.N. Steinmann, C. Corminboeuf, A generalized-gradient approximation exchange hole model for dispersion coefficients, J. Chem. Phys. 134 (2011) 44117–44122.
[63] S.N. Steinmann, C. Corminboeuf, Comprehensive Benchmarking of a Density-Dependent Dispersion Correction, J. Chem. Theory Comput. 7 (2011) 3567–3577.
[64] G. Kresse, D. Joubert, From ultrasoft pseudopotentials to the projector augmented-wave method, Phys. Rev. B 59 (1999) 1758–1775.
[65] M. Gajdoš, K. Hummer, G. Kresse, J. Furthmüller, F. Bechstedt, Linear optical properties in the projector-augmented wave methodology, Phys. Rev. B 73 (2006) 45112.
[66] D. Karhánek, T. Bučko, J. Hafner, A density-functional study of the adsorption of methane-thiol on the (111) surfaces of the Ni-group metals, J. Phys. Condens. Matter. 22 (2010) 265006–265015.
[67] P. Brüesch, Phonons: Theory and Experiments II: Experiments and Interpretation of Experimental Results, Springer, Berlin, Heidelberg, 1986.
[68] M. Digne, P. Sautet, P. Raybaud, P. Euzen, H. Toulhoat, Hydroxyl Groups on γ-Alumina Surfaces, J. Catal. 211 (2002) 1–5.
[69] M. Digne, P. Sautet, P. Raybaud, P. Euzen, H. Toulhoat, Use of DFT to achieve a rational understanding of acid-basic properties of γ-alumina surfaces, J. Catal. 226 (2004) 54–68.
[70] X. Krokidis, P. Raybaud, A.-E. Gobichon, B. Rebours, P. Euzen, H. Toulhoat, Theoretical Study of the Dehydration Process of Boehmite to γ-Alumina, J. Phys. Chem. B 105 (2001) 5121–5130.
[71] C. Arrouvel, H. Toulhoat, M. Breysse, P. Raybaud, Effects of P_{H2O}, P_{H2S}, P_{H2} on the surface properties of anatase-TiO_2 and γ-Al_2O_3: a DFT study, J. Catal. 226 (2004) 260–272.
[72] G. Henkelman, G. Jóhannesson, H. Jónsson, Methods for Finding Saddle Points and Minimum Energy Paths 269–302.
[73] G. Henkelman, B.P. Uberuaga, H. Jónsson, A climbing image nudged elastic band method for finding saddle points and minimum energy paths, J. Chem. Phys. 113 (2000) 9901–9904.
[74] D. Sheppard, R. Terrell, G. Henkelman, Optimization methods for finding minimum energy paths, J. Chem. Phys. 128 (2008) 134106–134116.
[75] A. Heyden, A.T. Bell, F.J. Keil, Efficient methods for finding transition states in chemical reactions: Comparison of improved dimer method and partitioned rational function optimization method, J. Chem. Phys. 123 (2005) 224101–224115.
[76] Paul Fleurat-Lessard, Opt'n Path, http://pfleurat.free.fr/ReactionPath.php.
[77] R.A. Angnes, mechaSVG, 2020, https://github.com/ricalmang/mechaSVG.
[78] K.S. Liang, S.P. Cramer, D.C. Johnston, C.H. Chang, A.J. Jacobson, J.P. deNeufville, R.R. Chianelli, Amorphous MoS_3 and WS_3, J. Non-Cryst. Solids 42 (1980) 345–356.

[79] S.J. Hibble, G.B. Wood, Modeling the structure of amorphous MoS_3: a neutron diffraction and reverse Monte Carlo study, J. Am. Chem. Soc. 126 (2004) 959–965.
[80] S.J. Hibble, M.R. Feaviour, M.J. Almond, Chemical excision from amorphous MoS_3; a quantitative EXAFS study, J. Chem. Soc., Dalton Trans. (2001) 935–940.
[81] Y. Deng, L.R.L. Ting, P.H.L. Neo, Y.-J. Zhang, A.A. Peterson, B.S. Yeo, Operando Raman Spectroscopy of Amorphous Molybdenum Sulfide (MoS_x) during the Electrochemical Hydrogen Evolution Reaction, ACS Catal. 6 (2016) 7790–7798.
[82] H. Jiao, Y.-W. Li, B. Delmon, J.-F. Halet, The Structure and Possible Catalytic Sites of Mo_3S_9 as a Model of Amorphous Molybdenum Trisulfide, J. Am. Chem. Soc. 123 (2001) 7334–7339.
[83] S.J. Hibble, R.I. Walton, D.M. Pickup, A.C. Hannon, Amorphous MoS_3, J. Non-Cryst. Solids 232-234 (1998) 434–439.
[84] D. Genuit, I. Bezverkhyy, P. Afanasiev, Solution preparation of the amorphous molybdenum oxysulfide $MoOS_2$ and its use for catalysis, J. Solid State Chem. 178 (2005) 2759–2765.
[85] A. Müller, E. Diemann, E. Krickemeyer, H.J. Walberg, H. Bögge, A. Armatage, $[Mo_3(IV)S(S_2)_6]^{2-}$ from amorphous MoS_3 by the reaction with OH^- and R= 0.015 strucutre of $(NH_4)_2[Mo_3(IV)S(S_2)_6]$., Eur. J. Solid State Inorg. Chem. 30 (1993) 565–572.
[86] F.Z. Chien, S.C. Moss, K.S. Liang, R.R. Chianelli, Local and intermediate-range structure of amorphous MoS_3, Phys. Rev. B 29 (1984) 4606–4615.
[87] P.-Y. Prodhomme, P. Raybaud, H. Toulhoat, Free-energy profiles along reduction pathways of MoS_2 M-edge and S-edge by dihydrogen, J. Catal. 280 (2011) 178–195.